# Solid-Solution Nanoparticles: Use of a Nonhydrolytic Sol−Gel Synthesis To Prepare $HfO_2$ and $Hf_xZr_{1-x}O_2$ Nanocrystals

Jing Tang,[†,‡] Jason Fabbri,[‡,§] Richard D. Robinson,[‡,||] Yimei Zhu,[⊥] Irving P. Herman,[‡,||] Michael L. Steigerwald,*[,†,‡] and Louis E. Brus*[,†,‡]

*Department of Chemistry, Department of Applied Physics and Applied Mathematics, and Materials Research Science and Engineering Center, Columbia University, New York, New York 10027, and Materials Science Department, Brookhaven National Laboratory, Upton, New York 11973*

*Received January 9, 2004*

A nonhydrolytic sol−gel process closely following that of Hyeon et al. for the synthesis of $ZrO_2$ nanocrystals (*J. Am. Chem. Soc.* **2003**, *125*, 6553−6557) was used to synthesize highly crystalline and monodisperse $HfO_2$ nanoparticles. Reactions of hafnium isopropoxide with hafnium halides at high temperature in a strongly coordinating solvent yield nanometer-sized particles of $HfO_2$. The size, shape, and crystalline phase of the hafnia particles depend on both the reaction temperature and the halide. The nonhydrolytic cross-condensation method was also extended to the binary metal oxides nanocrystals, i.e., $HfO_2$−$ZrO_2$, $ZrO_2$−$TiO_2$, and $HfO_2$−$TiO_2$. Efforts to prepare nanocrystals of $Hf_xZr_{1-x}O_2$ over a wide range of $x$ were successful; however, this method could not be used to prepare either $Zr_xTi_{1-x}O_2$ or $Hf_xTi_{1-x}O_2$. In conjunction with X-ray powder diffraction and high-resolution transmission electron microscopy, Raman spectroscopy identifies the structural phase of the nanocrystals and also proves the formation of the Hf−Zr solid solution nanoparticles via the cross-condensation method. In the case of $Hf_xZr_{1-x}O_2$, for $x < 0.5$, highly monodisperse, roughly spherical particles of tetragonal $Hf_xZr_{1-x}O_2$ were formed, while for $x > 0.5$, small nanorods of the monoclinic phase of the binary oxide were obtained.

## Introduction

Transition metal oxides are widely used in many important technological applications such as solar energy conversion,[2] catalysis,[3] magnetic recording,[4] sensors,[5] and ceramics.[6] Yet compared to the intensive study of nanocrystals of semiconductors and metals, relatively little work has been done on the metal oxides. In this investigation we extend the synthetic methodology of this class of materials to include binary solid solutions of chemically similar oxides.

$HfO_2$ and $ZrO_2$ are called twin oxides, as they are similar in many chemical and physical properties. The resemblance is attributed to their similar crystal structure, which in turn is due to the lanthanide contraction characteristic of the third transition series—the ionic radii of $Hf^{4+}$ and $Zr^{4+}$ are 0.78 Å and 0.79 Å, respectively, despite their large difference in the atomic number. Both oxides are very important ceramic materials due to their large dielectric constants ($\epsilon_{hafnia} \sim 30$, $\epsilon_{zirconia} \sim 25$), high melting points (2758 and 2700 °C, respectively), and great chemical stabilities. As high K dielectrics, they and their $SiO_2$ solid solutions are highly promising replacements for $SiO_2$ as the gate dielectrics in metal-oxide−semiconductor devices to increase the film thickness and reduce the leakage current.[7] They are also widely used as heat-resistant, highly reflective, protective optical coatings[8] and in a number of other important technologies such as catalysis and oxygen sensors.

Hafnia and zirconia in the bulk can each adopt three different, albeit related, crystal structures at ambient pressures, i.e., monoclinic, tetragonal, and cubic. In the bulk each oxide is stable in the monoclinic phase at room temperature and each transforms to tetragonal at high temperatures, the former at 1720 °C and the latter at

* To whom correspondence should be addressed. E-mail: msteiger@chem.columbia.edu (M.L.S.) and brus@chem.columbia.edu (L.E.B.).
† Department of Chemistry, Columbia University.
‡ Materials Research Science and Engineering Center Columbia University.
§ MRSEC REU student from Fairfield University.
|| Department of Applied Physics and Applied Mathematics, Columbia University.
⊥ Materials Science Department, Brookhaven National Laboratory.

(1) Joo, J.; Yu, T.; Kim Y. W.; Park, H. M. Wu, F.; Zhang, J. Z.; Hyeon, T. *J. Am. Chem. Soc.* **2003**, *125*, 6553−6557.
(2) O'Regan, B.; Grätzel, M. *Nature* **1991**, *353*, 737.
(3) Zhang, Z.; Wang, C. C.; Zakaria, R.; Ying, J. Y. *J. Phys. Chem. B* **1998**, *102*, 10871.
(4) Raj, K.; Moskowitz, R. *J. Magn. Magn. Mate*r. **1990**, *8*5, 233.
(5) León, C.; Lucía, M. L.; Santamaría, J. *Phys. Rev. B* **1997**, *55*, 882.
(6) Garvie, R. C.; Hannink, R. H.; Pascoe, R. T. *Nature* **1975**, *258*, 703.
(7) Wilk, G. D.; Wallace, R. M.; Anthony, J. M. *J. Appl. Phys.* **2001**, *89*, 5243.
(8) Magunov, I. R.; Magunov, R. L.; Kornitskiy, G. P. *Funct. Mater.* **2001**, *8*, 563−565. Chow, R.; Falabella, S.; Loomis, G. E.; Rainer, F.; Stolz, C. J.; Kozlowski, M. R. *Appl. Opt.* **1993**, *32*, 5567; Waldorf, A. J.; Dobrowolski, J. A.; Sullivan, B. T.; Plante, L. M. *Appl. Opt*. **1993**, *32*, 5583.

10.1021/cm049945w CCC: $27.50 
Published on Web 03/11/2004

1170 °C.[9] At even higher temperatures (2600 and 2370 °C, respectively) the tetragonal phases transform to the cubic. The corresponding hafnia and zirconia phases are isomorphic, and therefore, at least in the bulk, they can form solid solutions, $Hf_xZr_{1-x}O_2$, over the complete concentration range ($0 < x < 1$).

$HfO_2$ has been less studied in the form of nanomaterials than its twin oxide $ZrO_2$. To the best of our knowledge, the synthesis of $HfO_2$ nanocrystals has been only briefly reported once,[10] to make planar waveguides. Those authors used the hydrolysis of hafnium oxychloride in ethanol to prepare nanocrystalline hafnia. The resulting $HfO_2$ nanocrystals were polydisperse ($4 \pm 1.5$ nm in diameter) and their crystalline phase was determined to be monoclinic only by the observation of the lattice plane (111) from high-resolution transmission electron microscopy. Here we extend the recently developed nonhydrolytic sol−gel method, with which $TiO_2$[11] and $ZrO_2$[1] nanocrystals have been successfully synthesized, to $HfO_2$ nanocrystals. This method was derived from the known chemistry of reaction of a metal halide with a metal alkoxide acting as the oxygen donor. In this reaction, the condensation between M−X and M−O−R forms the M−O−M bridge with the elimination of alkyl halide, as shown in eq 1:

$$\equiv M-X + \equiv M-O-R \rightarrow \equiv M-O-M\equiv + R-X \quad \text{(condensation)} \quad (1)$$

Various metal oxides such as $TiO_2$ and $Al_2O_3$ have been made via this reaction route in the bulk.[12] This reaction was first applied to make $TiO_2$ nanocrystals by Colvin and co-workers,[11] who found that when titanium chloride is injected into a solution of titanium isopropoxide in hot heptane in the presence of trioctylphosphine oxide (TOPO), 7.3-nm anatase $TiO_2$ nanocrystals form. The use of the coordinating TOPO solvent at high temperature was originally employed in the controlled synthesis of crystalline semiconductor nanocrystals.[13] Very recently, Heyon and co-workers[1] showed that the reaction between zirconium(IV) isopropoxide and zirconium(IV) chloride in pure TOPO at 340 °C generates highly monodisperse 4-nm tetragonal zirconia nanoparticles. Here we report that the reaction of hafnium isopropoxide with hafnium halides in the presence of coordinating ligands yields crystalline $HfO_2$ nanoparticles whose size and phase depend on the preparative conditions used.

Furthermore, we extend this nonhydrolytic sol−gel method to the binary metal oxide systems, i.e., $HfO_2$−$ZrO_2$, $ZrO_2$−$TiO_2$, and $HfO_2$−$TiO_2$ nanocrystals. It has been shown that in bulk ceramic preparations, cross-condensation between metal alkoxides and metal chlorides can produce binary metal oxides (eq 2):

$$mMX_n + nM'(OR)_m \rightarrow M_mM'_nO_{nm} + nmRX \quad \text{(cross-condensation)} \quad (2)$$

The advantage of this sol−gel processing of mulitcomponent oxides over the conventional mixed powder method is the expected improved homogeneity.[14] However, due to the fast ligand exchange reaction between the metal alkoxides and metal halides that produces metal chloroalkoxides,[14] homo- as well as heterocondensations may occur.

$$MCl_n + M'(OR)_n \rightarrow MCl_{n-x}(OR)_x + M'Cl_x(OR)_{n-x}... \quad (3)$$

Therefore, the homogeneity of the binary oxides will be achieved only when both condensations take place at similar rates. Systems such as $ZrO_2$−$TiO_2$ and $Al_2O_3$−$TiO_2$ have been studied in the bulk.[14] We will describe below how in the nanocrystal systems we find that the titanium alkoxides and chlorides are apparently much more reactive than the Zr and Hf reactants, and consequently, the desired $ZrTiO_4$ and $HfTiO_4$ are not obtained, but instead, self-condensation of the Ti reagents occurs, giving only anatase $TiO_2$. However, the similarity between the Hf and Zr allows for the successful synthesis of $Hf_xZr_{1-x}O_2$ nanocrystals with different morphologies and crystallinities through this cross-condensation method.

## Experimental Section

**General.** Unless otherwise noted, all synthesis operations were conducted under an inert atmosphere using standard techniques. Hafnium(IV)/zirconium (IV) isopropoxide propanol complex (Hf/Zr•$[OCH(CH_3)_2]_4$•$(CH_3)_2CHOH$, Strem Chemicals Inc., 99%); titanium(IV) isopropoxide ($Ti[OCH(CH_3)_2]_4$, Strem, 98%); hafnium(IV) chloride, zirconium(IV) chloride, and titanium (IV) chloride ($HfCl_4$, $ZrCl_4$ and $TiCl_4$, Aldrich Chemical Co., 99.9%, 99.9% and 99.8% respectively); and hafnium bromide and zirconium bromide ($HfBr_4$ and $ZrBr_4$,Aldrich, 99.99% and 99.8% respectively) were used as received without further purification. Trioctylphosphine oxide (TOPO, Aldrich Chemical Co., 99%) was degassed before use by several freeze−pump−thaw cycles. Low-resolution transmission electron microscopy (TEM) was performed using a JEOL 100cx microscope (accelerating voltage 100 kV). Higher resolution structural characterization of the nanoparticles was carried out using a field emission transmission electron microscope (JEOL3000F) operated at 300 kV. The instrument has a high-resolution polepiece with a point-to-point resolution of 0.16 nm. The high-resolution images presented in this paper were recorded using a CCD camera. Diffraction analysis for indexing and lattice parameter measurement was conducted for individual particles via fast Fourier transform of the images based on the computer code developed at Brookhaven National Laboratory. X-ray powder diffraction (XRD) was recorded using a Scintag x2 diffractometer. The elemental composition of the binary metal oxides nanoparticle samples was estimated using energy-dispersive X-ray spectroscopy (EDS, LEO 1455 UP scanning electron microscope) and more accurately determined by inductively coupled plasma (ICP) analysis (Desert Analytics, Tucson, AZ).

Raman scattering was performed in a backscattering configuration using the 325-nm line of a continuous wave helium−cadmium laser (Omnichrome). (Background luminescence in the samples prevented Raman signals to be discernible using 457.9-, 488-, and 514.5-nm wavelengths from an argon ion laser.) The beam was focused to a spot size of ~2 $\mu$m and incident power was less than 1 mW, to minimize heating in

(9) Cardarelli, F. *Materials Handbook;* Springer: London, 2000.
(10) Ribeiro, S. J. L.; Messaddeq, Y.; Goncalves, R. R.; Ferrari, M.; Montagna, M.; Aegerter, M. A. *Appl. Phys. Lett.* **2000**, *77*, 3502.
(11) Trentler, T. J.; Denler, T. E.; Bertone, J. F.; Agrawal, A.; Colvin, V. L. *J. Am. Chem. Soc.* **1999**, *121*, 1613.
(12) Vioux, A. *Chem. Mater.* **1997**, *9*, 2292.
(13) Murray, C. B.; Norris, D. J.; Bawendi, M. G. *J. Am. Chem. Soc.* **1993**, *115*, 8706; Katari, J. E. B.; Colvin, V. L.; Alivisatos, A P. *J. Phys. Chem.* **1994**, *98*, 4109.
(14) Andrianainarivelo, M.; Corriu, R. J. P.; Leclercq, D.; Mutin, P. H.; Vioux, A. *J. Mater. Chem.* **1997**, *7*, 279. Andrianainarivelo, M.; Corriu, R. J. P.; Leclercq, D.; Mutin, P. H.; Vioux, A. *J. Sol−Gel Sci. Technol.* **1997**, *8*, 89.

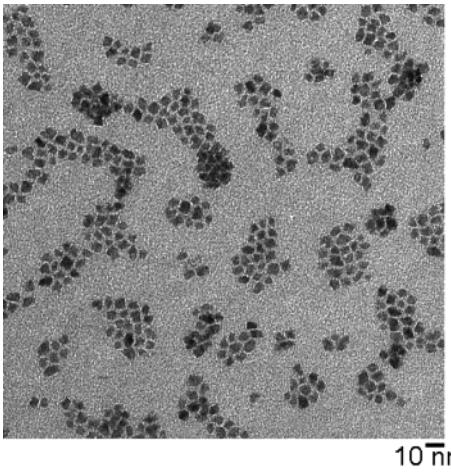


**Figure 1.** TEM image of the 5.5-nm $HfO_2$ nanocrystals.

the samples. A 0.6-m triple spectrometer (SPEX 1877, Triplemate) in subtractive configuration was used to collect and disperse the spectra, and a UV-coated CCD array detector (SPEX Spectrum One) recorded the spectra. Spectral calibration lamps (Oriel) were used to calibrate the 100−800 $cm^{-1}$ frequency range (resolution ~ 2 $cm^{-1}$). All peak intensity and position assignments are the result of Lorentzian fitting. Any small luminescence background was subtracted before determining peak widths and positions. All spectra were recorded at room temperature.

**Preparation of $HfO_2$ Nanocrystals.** The synthesis of $HfO_2$ employed here closely follows that of Hyeon et al. in their synthesis of $ZrO_2$.[1] ($Hf[OCH(CH_3)_2]_4$•$(CH_3)_2CHOH$ (2 mmol, 0.95 g) and $HfCl_4$ (2 mmol, 0.65 g) were added to 10 g (25.9 mmol) of degassed TOPO under argon. The reaction mixture was heated quickly to the ultimate process temperature and held at this temperature for 2 h with vigorous stirring. As the TOPO melted the inorganic reagents dissolved, giving initially a pale yellow solution and ultimately a thick white suspension. The reaction mixture was then cooled to ~ 60 °C and acetone was added to precipitate the hafnia nanoparticles. The precipitate was retrieved by centrifugation and washed several times with acetone to remove excess TOPO. The particles are capped with TOPO ligands and can be readily redispersed in hexane, producing a colorless solution. Results of complete elemental analysis (C, H, P, Hf, Zr, Cl; Desert Analytics, Tucson, AZ) were consistent with TOPO-capped metal oxide nanoparticles. Traces (~1 atom %) of residual chlorine were typical.

**Preparation of $Hf_xZr_{1-x}O_2$ Nanocrystals.** For the synthesis of $Hf_xZr_{1-x}O_2$ nanocrystals, various molar ratios of $M(O^iPr)_4$ to $M'Cl_4$ (M, M′ representing Hf and/or Zr) were used. In view of eq 2 above, the reactions must be balanced by equalizing the amounts of total isopropoxide and chloride species. For example, when $[Hf(O^iPr)_4]/[ZrCl_4] = 2$ is used, 1 equivalent of $HfCl_4$ is added in order to ensure that the amount of chloride equals the amount of alkoxide. In this case, the initial Hf/Zr is thus 3, while the initial isopropoxide/chloride ratio is 1. The mixed-oxide nanoparticle synthesis was conducted in the same manner as in the $HfO_2$ synthesis. Again, a pale yellow solution formed at the beginning of the reaction and a thick white or sometimes blue suspension formed by the completion of the reaction. In addition to TEM and XRD, the nanoparticles, capped by TOPO, were characterized by EDS and ICP analysis to determine the elemental composition.

## Results and Discussion

**$HfO_2$ Nanocrystals.** When $HfCl_4$ and $Hf(O^iPr)_4$ are allowed to react at 360 °C in neat TOPO, $HfO_2$ nanoparticles form in solution. In Figure 1 we show a TEM micrograph of this material, and in Figure 2 we show its XRD pattern. These data indicate that the $HfO_2$

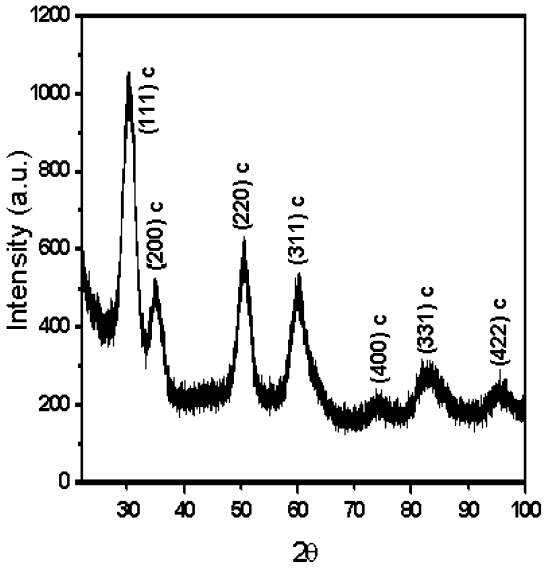


**Figure 2.** XRD pattern of the 5.5-nm $HfO_2$ nanocrystals.

nanoparticles are quite faceted and monodisperse. Due to their faceted shape, it is cumbersome to characterize the size of these particles, but if we approximate them as spheres, the average particle diameter determined is 5.5 nm. Particle sizes measured by TEM are in general agreement with the XRD determinations. The nanoparticles are highly crystalline, as judged both from the XRD and Selected Area Electron Diffraction (SAED, see the Supporting Information). As in the case of the recently reported tetragonal $ZrO_2$ nanocrystals,[1] all the diffraction peaks can be assigned to a cubic structure; however, since the tetragonal phase of $HfO_2$ is only slightly distorted from the cubic phase (for bulk $HfO_2$, the *c*/*a* ratio is only 1.02, very close to the cubic value of 1.0) and since the peaks are broadened due to the small crystallite size, it is very difficult to distinguish between these two crystal phases from the diffraction data. Nevertheless, the diffraction pattern indicates that the nanoparticles are formed in either the tetragonal or cubic forms. The Raman spectrum (Figure 3, trace b) does distinguish between the two phases. In cubic hafnia (yttrium stabilized), only a single peak at 620 $cm^{-1}$ is seen,[15] which is not the case for our samples. The peak near 276 $cm^{-1}$ (labeled T2) is particularly distinctive in the tetragonal phase and is seen here, so we conclude that the $HfO_2$ particles are formed predominantly in the tetragonal phase.

However, there are very weak peaks in the XRD patterns that suggest the presence of a lower symmetry phase. This is confirmed by the Raman spectrum that shows peaks that are characteristic of the monoclinic phase (peaks labeled M). Therefore, $HfO_2$ also forms in the monoclinic modification, although only in small amounts.

When this reaction is conducted at 400 °C, the $HfO_2$ forms as nanorods, as shown in Figure 4. These nanorods have a small aspect ratio, 2.3, and they are about 7.6 nm in length and 3.4 nm in diameter. The crystalline phase of these nanorods is determined to be monoclinic from the XRD pattern (Figure 5). We find no similar

(15) Fujimori, H.; Yashima, M.; Sasaki, S.; Kakihana, M.; Mori, T.; Tanaka, M.; Yoshimura, M. *Chem. Phys. Lett.* **2001**, *346*, 217.

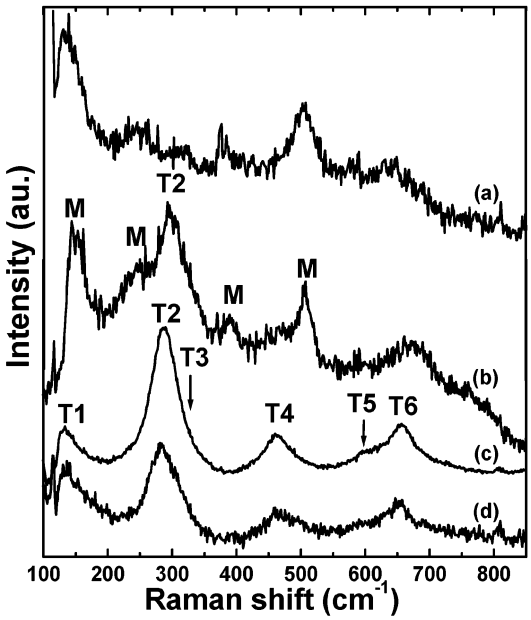


**Figure 3.** Room-temperature Raman spectra of nanoparticle hafnia−zirconia oxide solid solutions: (a) 3.7-nm $HfO_2$, (b) 5.5-nm $HfO_2$, (c) 4.3-nm $Hf_{0.45}Zr_{0.55}O_2$, and (d) 4.6-nm $Hf_{0.35}Zr_{0.65}O_2$. Labels T1−T6 identify the six tetragonal modes. Peaks labeled M identify the observed monoclinic modes.

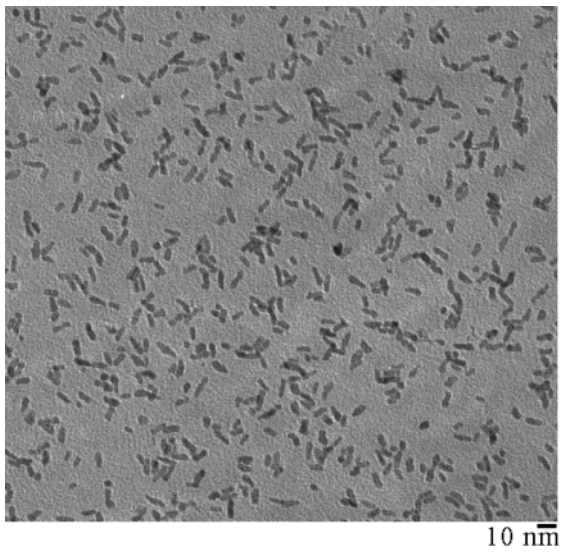


**Figure 4.** TEM image of the $HfO_2$ nanorods.

temperature effect in the $ZrO_2$ case: higher temperature affects neither the morphology nor the phase of the $ZrO_2$ nanocrystals.

When hafnium(IV) bromide is used as a precursor instead of hafnium chloride under otherwise identical conditions, the diameter of the hafnia nanoparticles decreases to 3.7 nm. The effect of the metal halide source compound on the characteristics of the nanoparticles ultimately formed was studied in both $TiO_2$[11] and $ZrO_2$[1] systems, and in each case it was shown that increased nucleophilicity (or size) of the halide results in smaller nanocrystals. As suggested by Colvin and coworkers,[11] the reaction rate of the alkyl halide elimination may play a role in the nucleation and growth of nanocrystals and thus the particle size and size distribution. Moreover, in the $HfO_2$ case not only does the size of the particles change, but so does the phase. The

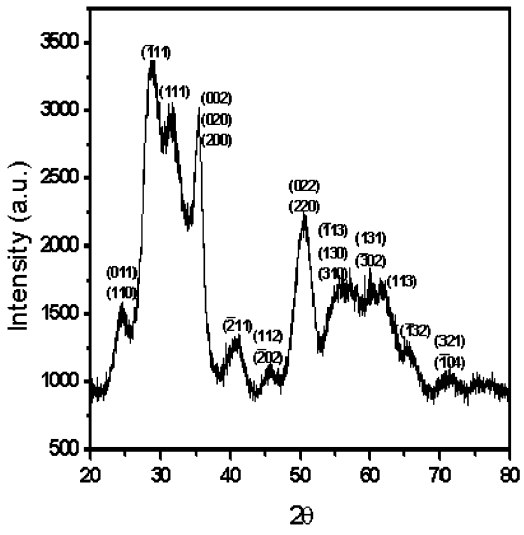


**Figure 5.** XRD pattern of the $HfO_2$ nanorods.

smaller, $HfBr_4$-based, hafnia particles form in the monoclinic structure, as determined from XRD and Raman scattering (Figure 3, trace a). Some phase change also occurred in the case of $TiI_4$ in the $TiO_2$ synthesis,[11] where some rutile phase was present in addition to the majority anatase phase.

As mentioned above, $HfO_2$ and $ZrO_2$ in the bulk are monoclinic at room temperature, although the tetragonal phase is more desirable in many important technology applications. To stabilize tetragonal or cubic $HfO_2$ and $ZrO_2$, divalent and trivalent cationic species such as $Mg^{2+}$, $Ca^{2+}$, $Cr^{3+}$, and $Y^{3+}$ must be incorporated.[16] It has been reported[17] that the stabilization of the crystalline phase of the solids can be strongly influenced by the dimensionality of the constituent particles; thus, the "high temperature" (that is, the higher symmetry) phase is observed in ceramic powders comprised of nanometer-sized grains. To stabilize pure tetragonal $ZrO_2$ at room temperature, the critical grain size was predicted to be less than 30 nm.[17] This is due to the lower surface free energy of the tetragonal form as compared to that of the monoclinic phase, which becomes more prominent for nanometer-sized particles. Therefore, from the thermodynamic point of view, the tetragonal phase should be even more strongly favored in the smaller $HfO_2$ nanoparticles (those arising from $HfBr_4$). However, in the present case the larger $HfO_2$ particles (formed from $HfCl_4$) are primarily tetragonal while the smaller ones (formed from $HfBr_4$) are monoclinic. This emphasizes the point that these processes are not simple.

**Binary Oxide Nanocrystals.** Mixtures of alkoxides and chlorides were used to make binary oxide $Hf_xZr_{1-x}O_2$ nanocrystals. When equimolar amounts of Hf and Zr species were used, i.e., either $Hf(O^iPr)_4$ with $ZrCl_4$ or $Zr(O^iPr)_4$ with $HfCl_4$, EDS measurements indicate the presence of both Hf and Zr in the product. The elemental ICP accurately determines the compositions of Hf and Zr, and it shows that the Zr/Hf elemental ratio in the product solid is always higher than in the initial reagent

(16) Ray, J. C.; Pramanik, P.; Ram, S. *Mater. Lett.* **2001**, *48*, 281; Hunter, O., Jr.; Scheidecker, R. W.; Tojo, S. *Mater. Sci. Monogr.* **1980**, *6*, 679.

(17) Garvie, R. C. *J. Phys. Chem.* **1965**, *69*, 1238; Garvie, R. C. *J. Phys. Chem.* **1978**, *82*, 218.

**Table 1. Summary of the Cross-Condensation Reactions That Produce $Hf_xZr_{1-x}O_2$ Nanocrystals[a]**

| reactions | Hf, Zr | phase[b] | size (nm) |
|---|---|---|---|
| $Hf(O^iPr)_4 + ZrCl_4$ | 0.45, 0.55 | t | 4.3 |
| $Hf(O^iPr)_4 + ZrBr_4$ | 0.40, 0.60 | t | 3.4 |
| $Zr(O^iPr)_4 + HfCl_4$ | 0.35, 0.65 | t | 4.6 |
| $Zr(O^iPr)_4 + HfBr_4$ | 0.36, 0.64 | t | 3.6 |
| $2Zr(O^iPr)_4 + HfCl_4 + ZrCl_4$ | 0.19, 0.81 | t | 5.1 |
| $3Zr(O^iPr)_4 + HfCl_4 + 2ZrCl_4$ | 0.12, 0.88 | t | 4.8 |
| $2ZrCl_4 + Hf(O^iPr)_4 + Zr(O^iPr)_4$ | 0.21, 0.79 | t | 5.2 |
| $3ZrCl_4 + Hf(O^iPr)_4 + 2Zr(O^iPr)_4$ | 0.11, 0.89 | t | 4.6 |
| $1.5Hf(O^iPr)_4 + ZrCl_4 + 0.5HfCl_4$ | 0.54,0.46 | m | $8.5 \times 3.6$ |
| $2Hf(O^iPr)_4 + ZrCl_4 + HfCl_4$ | 0.66, 0.33 | m | $11.2 \times 3.1$ |
| $3Hf(O^iPr)_4 + ZrCl_4 + 2HfCl_4$ | 0.75, 0.25 | m | $8.7 \times 3.4$ |
| $5Hf(O^iPr)_4 + ZrCl_4 + 4HfCl_4$ | 0.84, 0.16 | m | $11.3 \times 3.5$ |
| $2HfCl_4 + Zr(O^iPr)_4 + Hf(O^iPr)_4$ | 0.62, 0.38 | m | $8.0 \times 3.5$ |
| $3HfCl_4 + Zr(O^iPr)_4 + 2Hf(O^iPr)_4$ | 0.73, 0.27 | m | $11.2 \times 3.1$ |

[a] All the nanocrystals were characterized by elemental ICP, TEM, and XRD. [b] The t and m represent tetragonal and monoclinic, respectively.

mixture (Table 1). We interpret this as indicating the higher reactivity of the Zr species than the Hf species.

The amounts of C, H, and P in the samples were also determined from the elemental ICP measurements. For example, in the products from the reaction of $2Hf(O^iPr)_4 + ZrCl_4 + HfCl_4$, the measured weight percentage of C, H, and P are 9.86, 1.83, and 1.37%; that is, the C/H and C/P molar ratios are 2.13 and 18.7, respectively. As in most other cases, the C/H molar ratio is very close to that in TOPO (2.22); however, the C/P molar ratio is quite different from that in TOPO (24). This could suggest that TOPO decomposes a little bit at the high temperature used in the reactions. One thing we should also note is that the weight percentage of P in the samples is quite small, but the molecular weight of P is relatively large; thus, a small measured weight change of P can make a considerable change in these calculated ratios.

TEM shows that the particles made from either reaction are still faceted and monodisperse. Representative TEM images of particles from the reaction of $Hf(O^iPr)_4$ with $ZrCl_4$ at a ratio of 1:1 are shown in Figure 6. The high-resolution TEM image of a single particle (Figure 6b) clearly demonstrates all the facets of the particle, and the diffractogram (Fourier transformation of the image) of the same particle proves the single crystallinity of the particle. Not surprisingly, in view of the similarity of the lattice parameters of the two endpoint materials, the XRD patterns of the $Hf_xZr_{1-x}O_2$ particles are essentially identical to either tetragonal $HfO_2$ or $ZrO_2$ (see the Supporting Information). Similar to the cases of pure $HfO_2$ or $ZrO_2$ nanocrystals, it is difficult to differentiate between cubic and tetragonal phases of the binary oxide nanoparticles based just on the XRD patterns; however, the Raman spectra (Figure 3, trace c) show the $Hf_{0.45}Zr_{0.55}O_2$ nanocrystals to be tetragonal (see discussion below). When either $HfBr_4$ or $ZrBr_4$ is used instead of the corresponding chloride, the resulting particles are smaller (3.6 and 3.4 nm, respectively) but retain the tetragonal phase. Since the $ZrO_2$ nanocrystals from the $ZrBr_4$ reaction are tetragonal while the $HfO_2$ nanocrystals from $HfBr_4$ are monoclinic, this is evidence that Zr helps stabilize the $Hf_xZr_{1-x}O_2$ in the tetragonal phase.

To change $x$ in the $Hf_xZr_{1-x}O_2$ nanocrystals, different molar ratios of Hf and Zr precursors were used, always

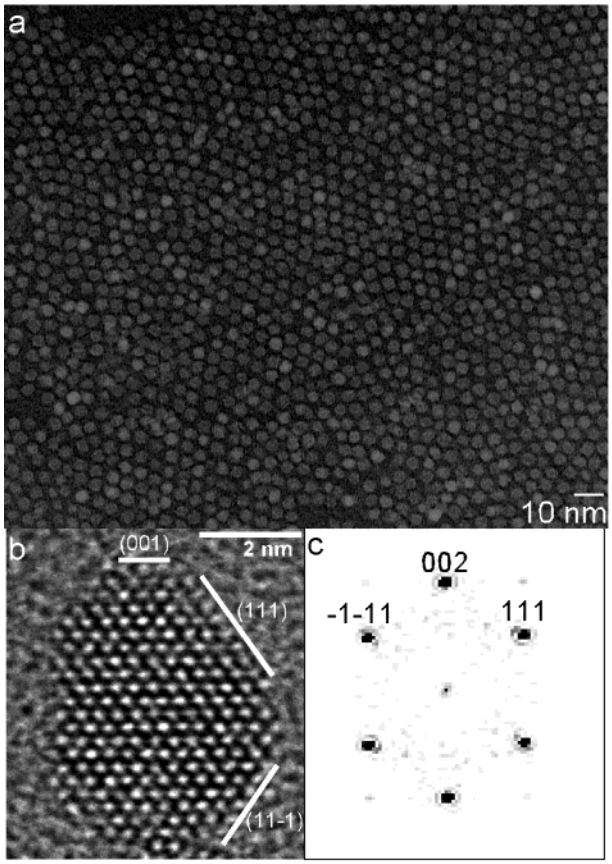


**Figure 6.** TEM images of the 4.3-nm $Hf_{0.45}Zr_{0.55}O_2$ nanocrystals from the reaction of $Hf(O^iPr)_4 + ZrCl_4$. (a) Low-resolution TEM image that shows the high monodispersity of the particles. (b) High-resolution TEM image of a single particle that clearly demonstrates the faceted nature of these particles and (c) diffractogram (Fourier transformation of the image) of the same particle that shows the single crystallinity of the particle. The high-resolution images were taken along the [110] zone axis.

balancing the total amounts of alkoxide and chloride. It was found that the chemical composition change is accompanied by changes in the particle morphology and phase. When the starting Zr/Hf ratio is 1 or greater, the product phase and morphology are similar to those of the pure Zr reaction, i.e., highly monodisperse, roughly spherical, tetragonal nanoparticles (similar to Figure 6). The reaction temperature does not have much effect on the morphology or phase of the particles. On the other hand, when the starting Zr/Hf ratio is less than 1, the reactions are similar to the reaction of pure $HfO_2$ in the sense that temperature does have an effect on the resulting nanocrystals. At 360 °C, the obtained particles are tetragonal but have irregular shape and a wide size distribution, while at higher temperature 400 °C small nanorods form, and as might be expected, the nanorods form in the monoclinic phase. In the Hf-rich reactions, the particles tend to grow into anisotropic nanorods. For example, Figure 7 shows representative TEM images of the nanoparticles produced in the reaction of $Hf(O^iPr)_4$, $HfCl_4$, and $ZrCl_4$ in the ratio of 2:1:1. From the low-resolution TEM image (Figure 7a), we can see that most of the particles are nanorods, while a very small number of them are roughly spherical. The nanorods display considerable distribution in length but reasonable uniformity in diameter. They are about 11.5 nm

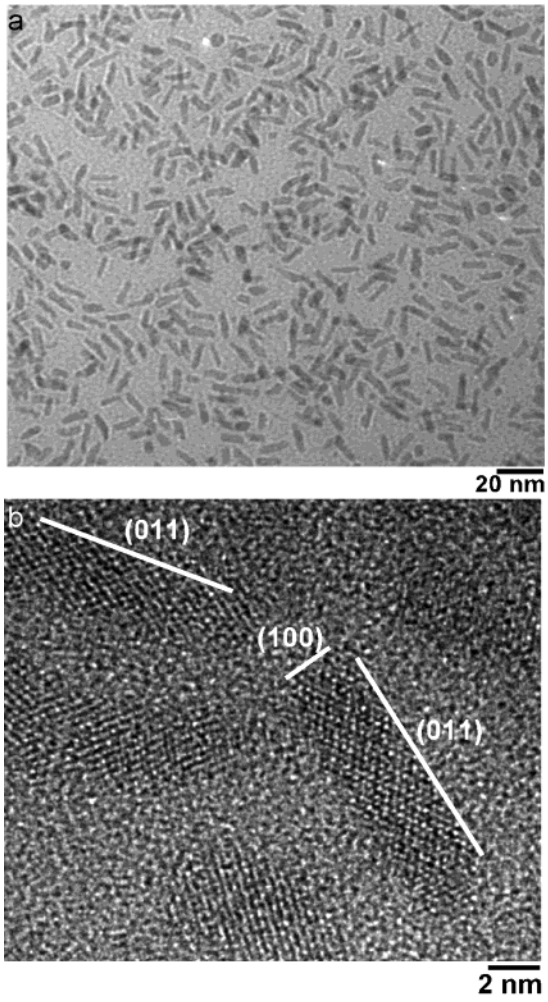


**Figure 7.** Low-resolution (a) and high-resolution (b) TEM images of the $Hf_{0.66}Zr_{0.34}O_2$ nanorods from the reaction of $2Hf(O^iPr)_4 + ZrCl_4 + HfCl_4$. The high-resolution TEM image determines the growth lattice planes of these nanorods to be (100).

in length and 3.1 nm in diamete, giving an average aspect ratio of about 3.6. From the high-resolution TEM image (Figure 7b), the growth lattice plane of these nanorods is determined to be (100) of the monoclinic phase, consistent with the XRD pattern (see the Supporting Information).

Table 1 summarizes the reactions with the resulting nanocrystals characterized by elemental composition, size, morphology, and crystalline phase. One should note that the symmetrical reactions of $M(O^iPr)_4/M'Cl_4$ or $MCl_4/M'(O^iPr)$ of same ratio, for example, $2Zr(O^iPr)_4 + HfCl_4 + ZrCl_4$ or $2ZrCl_4 + Hf((O^iPr)_4 + Zr((O^iPr)_4$, usually produce very similar results in terms of the chemical compositions of the nanocrystals.

All of the above discussion presupposes that each particle in the product ensemble is constitutionally similar. However, EDS, ICP, and XRD (owing to the similarity between the lattice parameters of zirconia and hafnia and the breadth of the diffraction lines dictated the nanometric particles) cannot prove that we have made nanoparticles of a solid solution material rather than simply mixtures of particles of pure zirconia and pure hafnia. Raman spectroscopy is particularly well-suited to discriminate between these two alternatives. Since Raman spectroscopy measures phonon frequencies, and since the phonon modes are localized in each particle, it is an excellent diagnostic of the ensemble average of the constitution of individual particles as opposed to merely the ensemble-averaged constitution.

The Raman spectra of tetragonal and monoclinic $Hf_xZr_{1-x}O_2$ samples are shown in Figure 3. The six modes allowed for the tetragonal phase (space group $D_{4h}$,[15] $Z = 2$) are clearly seen in the $Hf_{0.45}Zr_{0.55}O_2$ and $Hf_{0.35}Zr_{0.65}O_2$ samples (peaks labeled T1, T2, T3, T4, T5, and T6). Comparisons among these spectra indicate not only that the samples are of solid-solution particles (since there is no peak doubling) but also that the mixed-metal nanoclusters form in the tetragonal modification. The intensity of the fourth Raman mode around 461 $cm^{-1}$ has been used to identify the tetragonal and cubic phase boundary.[18] Its strength relative to the 654 $cm^{-1}$ mode classifies these samples unambiguously in the tetragonal region and not near the cubic phase boundary. Also shown in Figure 3 are Raman spectra of $HfO_2$ particles (traces a and b). The 3.7-nm $HfO_2$ particles show peaks at frequencies seen for monoclinic samples of the same composition (labeled M in the figure).

Similar reactions have also been tried with the $ZrO_2-TiO_2$ and $HfO_2-TiO_2$ systems. It is known that $ZrO_2$ and $HfO_2$ can form a binary metal oxide with $TiO_2$, i.e., $ZrTiO_4$ and $HfTiO_4$, respectively; these mixed oxides are used in catalysis, sensors, etc. The cross-condensation sol−gel method has been used to make $ZrTiO_4$ in the bulk and after calcination at 700 °C the gel indeed crystallizes directly into $ZrTiO_4$ without the intermediate formation of $ZrO_2$ or $TiO_2$.[14] However, when equal molar amounts of Zr/Hf and Ti species were used in an attempt to synthesize the binary metal oxides nanocrystals, EDS shows that there is always much more Ti than Zr or Hf. Correspondingly, only anatase $TiO_2$ pattern appears in the XRD. These results suggest the much higher reactivity of the Ti compounds than the Zr or Hf compounds.

## Conclusion

The nonhydrolytic sol−gel method is extended to $HfO_2$ nanocrystals. Reactions of hafnium isopropoxide with hafnium halides at high temperature in pure TOPO yield nanometer-sized $HfO_2$ particles whose size, shape, and crystalline phase depend on both the reaction temperature and the halide. For the first time, the nonhydrolytic cross-condensation method is used to make binary metal oxides nanocrystals. The cross-condensation of $Hf/Zr(O^iPr)_4$ and $Zr/HfCl_4$ generates highly monodisperse spherical tetragonal $Hf_xZr_{1-x}O_2$ nanocrystals and monoclinic nanorods, depending on the relative ratios of the precursors used in the reactions. In conjunction with XRD and high-resolution TEM, Raman spectroscopy not only resolves the phases of the as-prepared nanoparticles but also proves the formation of the Hf−Zr solid solution via the cross-condensation synthesis. Attempts to prepare $ZrTiO_4$ and $HfTiO_4$ were also made, but due to the much higher reactivity of the Ti compounds than the Zr and Hf compounds, only anatase $TiO_2$ with small amounts of $ZrO_2$ or $HfO_2$ were

(18) Yashima, M.; Takahashi, H.; Ohtake, K.; Hirose, T.; Kakihana, M.; Arashi, H.; Ikuma, Y.; Suzuki, Y.; Yoshimura, M. *J. Phys. Chem. Solids* **1996**, *57*, 289.

obtained. Overall, it is highly promising that this nonhydrolytic method can be used to synthesize additional metal oxides as well as mixed or doped metal oxides.

**Acknowledgment.** We would like to thank Dee Breger for the EDS measurements and Gertrude Neumark for the loan of the He−Cd laser. This work has been primarily supported by the NSF via the MRSEC Program (DMR-0213574) at Columbia University. R.D.R. was supported in part by the Ford Foundation.

**Supporting Information Available:** Electron diffraction of the 5.5-nm $HfO_2$ nanocrystals, XRD patterns of the $Hf_{0.45}Zr_{0.55}O_2$ nanoparticles and $Hf_{0.66}Zr_{0.34}O_2$ nanorods, and TEM image of the 3.4-nm $Hf_{0.40}Zr_{0.60}O_2$ nanocrystals. This material is available free of charge via the Internet at http://pubs.acs.org.

CM049945W